Non-specific binding of Na^+ and Mg^{2+} to RNA determined by force spectroscopy methods Supplementary Material

C. V. Bizarro[a,b,†,**], A. Alemany[a,b,**], F. Ritort[a,b,*]

[a]Departament de Física Fonamental, Universitat de Barcelona, Diagonal 647, 08028 Barcelona, Spain;

[b]CIBER-BBN de Bioingeniería, Biomateriales y Nanomedicina, Instituto de Sanidad Carlos III, Madrid, Spain;

†Present Address: Centro de Pesquisas em Biologia Molecular e Funcional/PUCRS Avenida Ipiranga 6681, Tecnopuc, Partenon 90619-900, Porto Alegre, RS, Brazil

*To whom correspondence should be addressed. Tel: +34-934035869; Fax: +34-934021149; Email: fritort@gmail.com, ritort@ffn.ub.es

**These authors contributed equally to the paper

Contents

S1 Molecules studied

[Mon^+] (mM)	[Mg^{2+}] (mM)	loading rate (pN/s)	Molecules	Total cycles
50	0	1.8	4	95
50	0	12.5	2	376
150	0	1.8	6	292
150	0	12.5	4	329
550	0	1.8	5	163
550	0	12.5	3	501
1050	0	1.8	9	185
1050	0	12.5	9	405
50	0.01	1.8	5	146
50	0.01	12.5	5	386
50	0.1	1.8	7	374
50	0.1	12.5	9	1434
50	0.5	1.8	2	112
50	0.5	12.5	2	533
50	1.0	1.8	4	205
50	1.0	12.5	6	2183
50	4.0	1.8	7	385
50	4.0	12.5	7	1112
50	10.0	1.8	7	190
50	10.0	12.5	3	1189

Table S1: Number of molecules and total cycles measured at each ionic salt condition.

S2 Study of fraying

The phenomenon of "fraying" at the ends of DNA and RNA duplexes can potentially interfere with both solution and single-molecule measurements of DNA and RNA stabilities, and it was previously suggested that its effects should be introduced in data analysis [1]. In order to check if fraying has an important role in our sequence, we computed the released (absorbed) molecular extension Δx_m in the unfolding (folding) process. This can be done using the expression:

$$\Delta x_m = \frac{\Delta f}{k_{\text{eff}}} \tag{S1}$$

where Δf is the force jump measured along the force-distance curve (FDC) and k_{eff} is its slope before the transition. The change in the molecular extension is also equal to:

$$\Delta x_m = x_N(f) - x_n(f) \tag{S2}$$

where $x_N(f)$ is the equilibrium end-to-end distance of the unzipped hairpin evaluated at the unfolding/folding force ($N = 20$ in this case); $x_n(f)$ is the projection of the folded hairpin along the force axis; and n denotes the number of open/frayed base pairs in the F state. Ideally, in the absence of fraying, $n = 0$. However, in presence of fraying we should find the value $n > 0$ such that eq. (S1) and (S2) give the same change in molecular extension.

From the FDC we obtain $\Delta f = 1.2 \pm 0.1$ pN and $k_{\text{eff}} = 0.0625 \pm 0.0146$ pN/nm which, using eq. (S1), gives $\Delta x_m = 19 \pm 2$ nm for any salt concentration. On the other hand, we evaluate $x_N(f)$ and $x_{n=0}(f)$ using the elastic properties summarized in Tables 1 and 2 at the measured unfolding/folding forces. Using eq. (S2) for $n = 0$ we obtain that predicted values for Δx_m lie in the range between 18.2 and 19.7 nm. Therefore, we conclude that fraying is not important for the molecule under study because the experimental evaluation of Δx_m (eq. (S1)) is in agreement with the estimation of the released molecular extension for $N = 20$ and $n = 0$.

The effect of fraying has been proved to play an important role in former single-molecule stretching experiments, like in Woodside *et. al.* [1]. To understand when fraying is relevant in RNA or DNA hairpins we can take a look to sequences at the beginning of the stem as a higher GC-content makes the structure more stable. For instance, the RNA hairpin studied here starts with 5'-GCG-3', whereas most sequences studied by Woodside *et al.* [1] start with 5'-GAG-3' (except two sequences that start with 5'-TAT-3' and 5'-AAG-3'). In Table S2 we compute the free energy difference $\Delta G_1(f)$ at 1 M NaCl between the completely folded conformation ($n = 0$) and the frayed configuration with one open distal base pair ($n = 1$) at different values of force for our RNA hairpin and molecule 20R55/4T in [1]. At zero force, $\Delta G_1^{20R55/4T}(0)$ is below 3 $k_{\text{B}}T$ and consequently thermal fluctuations can overcome the energetic barrier and the frayed conformation can take place. However, in the case of our hairpin ΔG_1 is too high for thermal fluctuations to overcome the energetic barrier. The same trend is observed at 10 pN. At 20 pN fraying is irrelevant because both molecules are in the unfolded state.

Motivated by solution measurements [2, 3], we also considered the possibility of fraying at the opposite end of the stem, on the base pairs closest to the loop. However, we found free energy differences of more than 10 $k_{\text{B}}T$ between these configurations and the closed configuration, and consequently we conclude that these "frayed" configurations are not affecting our results.

Based on these considerations, we conclude that fraying plays a rather minor role (if any) on the thermodynamics and kinetics of folding/unfolding of the RNA hairpin and can be neglected.

Force (pN)	$\Delta G_1^{20R55/4T}$ (k_BT)	ΔG_1^{RNA} (k_BT)
0	2.67	6.45
10	1.08	4.86
20	-1.34	2.45

Table S2: Free energy differences between frayed ($n = 1$) and completely closed structures ($n = 0$) of 20R55/4T hairpin [1] and our RNA hairpin at 1 M NaCl and different forces.

S3 Derivation of the effective barrier $\mathbf{B_{eff}^{KT}(f)}$

Here we derive the analytical expression for the effective barrier of a one-dimensional free energy landscape based on the work by Hyeon and Thirumalai [4].

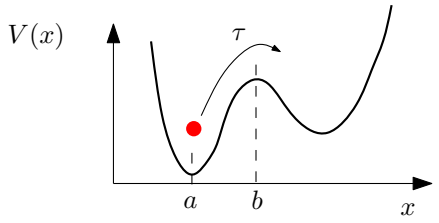

Figure S1: Brownian particle in a double well potential.

Suppose the system sketched in Fig. S1, where a Brownian particle is subject to the one dimensional potential $V(x)$. The time evolution of the probability density function (pdf) $p(x,t)$ to find the particle at the position x at time t follows the Fokker-Planck equation [4, 5]:

$$\begin{aligned}\frac{\partial p(x,t)}{\partial t} &= D\frac{\partial}{\partial x}\left[\frac{\partial}{\partial x}+\frac{1}{k_BT}\frac{dV(x)}{dx}\right]p(x,t)\\ &= D\frac{\partial}{\partial x}\left[e^{-\frac{V(x)}{k_BT}}\frac{\partial}{\partial x}e^{\frac{V(x)}{k_BT}}\right]p(x,t)\\ &= \mathcal{L}_{\mathrm{FP}}\left[p(x,t)\right]\end{aligned} \tag{S3}$$

Where D is the diffusion coefficient and $\mathcal{L}_{FP}$ is the Fokker-Plank operator. If we suppose that the particle initially is located at $x = a$, $p(x,0) = \delta(x-a)$, the formal solution of equation (S3) is:

$$p(x,t) = e^{t\mathcal{L}_{FP}}\delta(x-a) \tag{S4}$$

We want to evaluate the average time τ it takes to the Brownian particle to jump the kinetic barrier located at $x = b$. In order to simplify the following calculations, we suppose that there are absorbing conditions at $x = b$: once the particle reaches the maximum sketched in Fig. S1 it always goes to the right well. The probability to find the particle in the left well of the potential $V(x)$ ($x \in [-\infty, b]$) at time t, also known as the survival probability $S(t)$, can be defined as:

$$S(t) = \int_{-\infty}^{b} dx\ p(x,t) \tag{S5}$$

The time derivative of the survival probability is equal to the time survival pdf $\rho(t)$, that is, the

pdf of the time it takes to the Brownian particle to cross the barrier located at $x = b$.

$$S(t+dt) - S(t) = -\rho(t)dt \Rightarrow \rho(t) = -\frac{\partial S(t)}{\partial t} \tag{S6}$$

Therefore, the mean first passage time τ can be calculated as:

$$\begin{aligned}
\tau &= \int_0^\infty dt\ t\ \rho(b,t) \\
&= \int_0^\infty dt\ S(b,t) \\
&= \int_0^\infty dt \int_{-\infty}^b dx\ p(x,t) \\
&= \int_0^\infty dt \int_{-\infty}^b dx\ e^{t\mathcal{L}_{FP}}\delta(x-a) \\
&= \int_0^\infty dt \int_{-\infty}^b dx\ \delta(x-a)e^{t\mathcal{L}_{FP}^\dagger}1 \\
&= \int_0^\infty dt\ e^{t\mathcal{L}_{FP}^\dagger}1
\end{aligned} \tag{S7}$$

In order to obtain this expression we integrated by parts and used that the adjoint operator satisfies $f(x)\mathcal{L}\left[g(x)\right] = g(x)\mathcal{L}^\dagger\left[f(x)\right]$. If we apply the adjoint Fokker-Plank operator $\mathcal{L}_{FP}^\dagger$ at both sides of equation (S7) we obtain:

$$\begin{aligned}
\mathcal{L}_{FP}^\dagger\tau &= \int_0^\infty dt\ \mathcal{L}_{FP}^\dagger e^{t\mathcal{L}_{FP}^\dagger}1 \\
&= \int_0^\infty dt\ \frac{de^{t\mathcal{L}_{FP}^\dagger}}{dt}1 \\
&= -1
\end{aligned} \tag{S8}$$

Which gives a differential equation for the survival time τ that depends on the adjoint Fokker-Plank operator.

It can be demonstrated that:

$$\mathcal{L}_{FP}^\dagger = De^{\frac{V(x)}{k_B T}}\frac{\partial e^{-\frac{V(x)}{k_B T}}}{\partial x}\frac{\partial}{\partial x} \tag{S9}$$

and we can write the following differential equation:

$$\mathcal{L}_{FP}^\dagger\tau(x) = De^{\frac{V(x)}{k_B T}}\frac{\partial}{\partial x}\left(e^{-\frac{V(x)}{k_B T}}\right)\frac{\partial}{\partial x}\tau(x) = -1 \tag{S10}$$

In order to solve eq. (S10) we use the absorbing boundary condition $\tau(b) = 0$ and the reflecting boundary $\frac{\partial\tau}{\partial x}|_{x=a} = 0$.

$$\tau(x) = \frac{1}{D}\int_x^b dy\ e^{\frac{V(y)}{k_B T}}\int_a^y dx e^{-\frac{V(x)}{k_B T}} \tag{S11}$$

Once we have evaluated the average survival time of the Brownian particle, we want to evaluate the effective barrier of the potential $V(x)$. Using the phenomenological Arrhenius approach [6] that

considers that the survival time depends on the exponential of the barrier we can write:

$$\tau \simeq e^{\frac{B_{\text{eff}}}{k_{\text{B}}T}} \Rightarrow B_{\text{eff}} = k_{\text{B}}T \log\left(\tau/\tau_0\right) \tag{S12}$$

$$B_{\text{eff}} = k_{\text{B}}T \log\left(\frac{1}{\tau_0 D}\int_x^b dy\; e^{\frac{V(y)}{k_{\text{B}}T}} \int_a^y dx e^{-\frac{V(x)}{k_{\text{B}}T}}\right) \tag{S13}$$

τ_0 is related to the diffusion time of the particle the along x axis. By discretization of equation (S13) we obtain the expression (7) of the main paper,

$$B_{\text{eff}}(f) = k_{\text{B}}T \log\left[\sum_{n=0}^{N} e^{\frac{\Delta G_{\text{n}}(f)}{k_{\text{B}}T}} \left(\sum_{n'=0}^{n} e^{-\frac{\Delta G_{\text{n}'}(f)}{k_{\text{B}}T}}\right)\right] \tag{S14}$$

Where ΔG_n is the potential energy $V(x)$ and where we considered that $D\tau_0 \simeq \mathcal{O}(1)$.

S4 Sensitivity of the data analysis

An experimental estimation of the kinetic barrier is obtained from the measured transition rates $k_U(f)$ and $k_F(f)$. From the unfolding transition rate, the estimator of the kinetic barrier is given by:

$$\frac{B_{\rm eff}^{(U)}(f)}{k_{\rm B}T} = \log k_0 - \log k_U(f) \tag{S15}$$

Where $\log k_0$ is a constant (equal to the logarithm of the attempt rate at zero force for the activated kinetics) and $\log k_U(f)$ is estimated from the measured unfolding rupture forces (see section 2.6 in the main paper).

On the other hand, from folding rupture forces the estimation of the kinetic barrier is:

$$\begin{aligned}\frac{B_{\rm eff}^{(F)}(f)}{k_{\rm B}T} &= \log k_0 - \log k_F(f) + \frac{\Delta G_{\rm N}(f)}{k_{\rm B}T} \\ &= \log k_0 - \log k_F(f) + \frac{\Delta G_{\rm N}(0)}{k_{\rm B}T} + \frac{\Delta G_{\rm N}^{ssRNA}(f)}{k_{\rm B}T} + \frac{\Delta G_{\rm N}^{d_0}(f)}{k_{\rm B}T} \\ &= \log k_0 - \log k_F(f) + \frac{\Delta G_{\rm N}(0)}{k_{\rm B}T} - \frac{\int_0^f x_{\rm N}^{ssRNA}(f')df'}{k_{\rm B}T} + \log\left[\frac{k_{\rm B}T}{fd_0}\sinh\left(\frac{fd_0}{k_{\rm B}T}\right)\right]\end{aligned} \tag{S16}$$

Where $\log k_0$ is the same constant as in eq. (S15) and $\log k_F(f)$ is obtained from the measured folding rupture forces. The term $\Delta G_{\rm N}(0)/k_{\rm B}T$ is another constant equal to the free energy of the RNA hairpin at zero force; $\int_0^f x_{\rm N}^{ssRNA}(f')df'$ is a force dependent term evaluated according to the model used to describe the elastic response of ssRNA (here we use the WLC model with a salt-dependent persistence length P); and the last term, $\log\left[\frac{k_{\rm B}T}{fd_0}\sinh\left(\frac{fd_0}{k_{\rm B}T}\right)\right]$, is evaluated using $d_0 = 2.0$ nm at any salt condition for the given force f (see section 2.3).

Typically, $\log k_0$ is unknown and either $\Delta G_N(0)/k_{\rm B}T$ is unknown and P is known (here, for monovalent salt conditions) or $\Delta G_N(0)/k_{\rm B}T$ is known and P is unknown (for mixed monovalent/Mg^{2+} conditions).

S4.1 Sensitivity of the method at determining $\Delta G_{\rm N}(0)$

For a given value of the persistence length P we can evaluate the kinetic barrier from experimental unfolding/folding rupture forces by ignoring the unknown constants ($\log k_0$ and $\Delta G_N(0)/k_{\rm B}T$) and we obtain the result shown in Fig. S2A. Error bars are evaluated using the bootstrap method.

In order to determine the constant $\Delta G_N(0)/k_{\rm B}T$, *i. e.* the free energy of formation of the RNA hairpin, we impose the continuity of the kinetic barrier in folding and unfolding data (Fig. S2B). The error committed in the evaluation of $\Delta G_N(0)/k_{\rm B}T$ mainly depends on the good agreement of the overlapping between $\left(B_{\rm eff}^{(U)}(f) - \log k_0\right)$ and $\left(B_{\rm eff}^{(F)}(f) - \log k_0\right)$ and their error bars. In the example provided in Fig. S2B the best overlapping is found at $\Delta G_N(0) = 64\ k_{\rm B}T$. In the insets we see that the continuity requirement worsens for values of $\Delta G_N(0)$ as close as 64.4 or 63.6 $k_{\rm B}T$. As a consequence, we estimate $\Delta G_N(0) = 64.0 \pm 0.4\ k_{\rm B}T$ (see Table 1 in the main document).

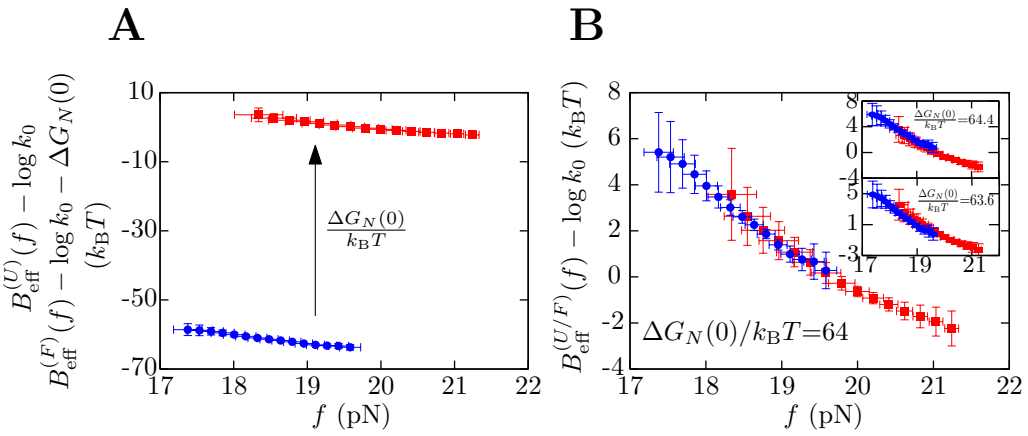

Figure S2: **Determination of $\Delta G_N(0)$.** Data obtained at 1.8 pN/s and 550 mM [Mon$^+$]. **(A)** Evaluation of $B^{(U)}(f) - \log k_0$ (red squares) and $B^{(F)}(f) - \log k_0 - \Delta G_N(0)/k_{\rm B}T$ (blue circles). **(B)** $\Delta G_N(0)/k_{\rm B}T$ is obtained using the overlapping of the kinetic barrier with force. Once unfolding and folding data overlap, the resulting experimental curve is equal to $B_{\rm eff}(f) - \log k_0$. *Insets*: The value of $\Delta G_N(0)/k_{\rm B}T$ can be overestimated (top) or underestimated (bottom) so that the continuity requirement is not well-satisfied.

S4.2 Sensitivity of the method at determining $\log k_0$

In order to estimate the attempt rate at zero force we need a theoretical model for the kinetic barrier. In the case of this work we use the Kramers theory (see section S3). Once we have evaluated $B_{\rm eff}(f) - \log k_0$, $\log k_0$ is obtained by overlapping the theoretical model to the experimental results, as shown in Fig. S3. The sensitivity in the determination of $\log k_0$ is similar to the sensitivity in determining $\Delta G_N(0)$: at $\log k_0$=10.5 we find the best match, and for values 0.4 greater or smaller the result significantly worsens (insets in Fig. S3B).

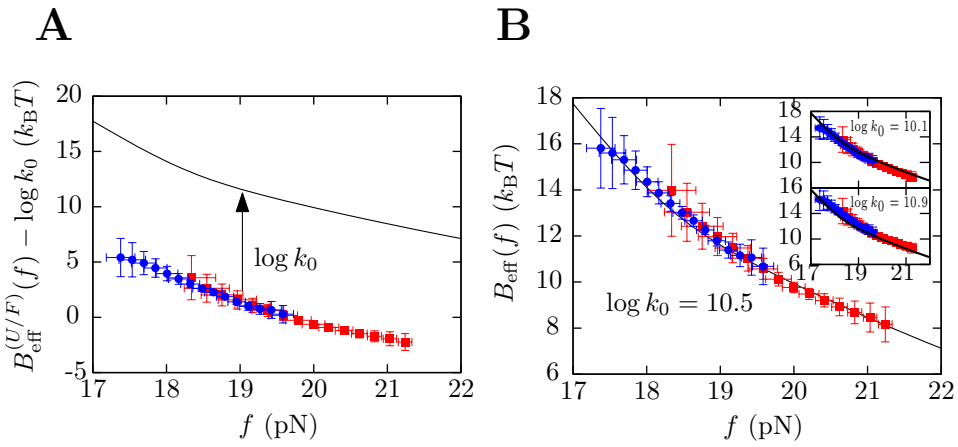

Figure S3: **Determination of $\log k_0$.** Data obtained at 1.8 pN/s and 550 mM [Mon$^+$]. **(A)** Black-straight line is the theoretical evaluation of the kinetic barrier using Kramers theory (section S3 and section 2.5 in the main document) and blue circles (red squares) are the experimental estimation of the kinetic barrier without the contribution of $\log k_0$ using folding (unfolding) rupture forces. **(B)** $\log k_0$ is obtained overlapping the experimental data to the theoretical curve. *Insets*: The value of $\log k_0$ can be underestimated (top) or overestimated (bottom) leading to a worse match between theory and experiments.

S4.3 Sensitivity of the method at determining P

The elastic contribution to $B_{\rm eff}(f)$ only applies to folding data, eq. (S16), and regulates the slope of the experimental estimation of the kinetic barrier in the range of experimentally measured folding forces. In this work we determine the persistence length P of ssRNA by comparing the profile of the kinetic barrier estimated from experimental data with the one evaluated using the Kramers theory (see Fig. S4). The sensitivity at determining P is limited by the determination of $\Delta G_N(0)/k_{\rm B}T$, $\log k_0$ and the error bars estimated for $B_{\rm eff}^{(U/F)}(f)$. Therefore, the is a feedback in the determination of the $\Delta G_N(0)/k_{\rm B}T$, $\log k_0$ and P: optimal values are those that give a best fit between experimental and theoretical estimations of the kinetic barrier.

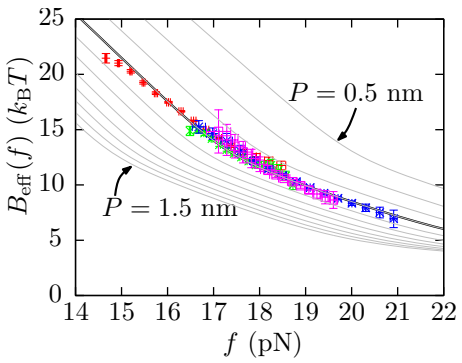

Figure S4: **Determination of P.** Data obtained at 1 mM [Mg^{2+}]. Gray lines are evaluations of the kinetic barrier using Kramers theory, eq. (S14), for different values of the persistence length ($P = 0.5, 0.6, 0.7, \ldots, 1.5$ nm). Experimental data is analyzed using also different values of the persistence length. In this case, at $P = 0.8 \pm 0.1$ nm we obtain the best overlapping between theory and experiments.

The same methodology was used to determine the value of m in the non-specific correction for the free energy of formation of one base pair, where the elastic parameters are known but the free energy is unknown (see section 3.5 and Fig. 4 in the main paper): we look for the best matching between theory and experiments.

S5 UV Absorbance experiments

In order to determine the effect of salt on the stability of the hairpin we obtained the melting profile of the molecule using UV absorbance at 260 nm. The melting temperature was measured at 70±1°C using a buffer containing 100 mM Tris.HCl, 1 mM EDTA and no NaCl neither $MgCl_2$. Results can be observed in Fig. S5A. We calculated the first derivative of the absorbance as a function of temperature (Fig. S5B) and observed several maximums along the resulting profile (see arrows), which denote the presence of pre-melted states. For instance, regions with a richer A-U content in the middle of the stem may dissociate before the whole hairpin is unfolded (Fig. S5C). This result invalidates the two-states assumption used to extract thermodynamic parameters from the melting curve.

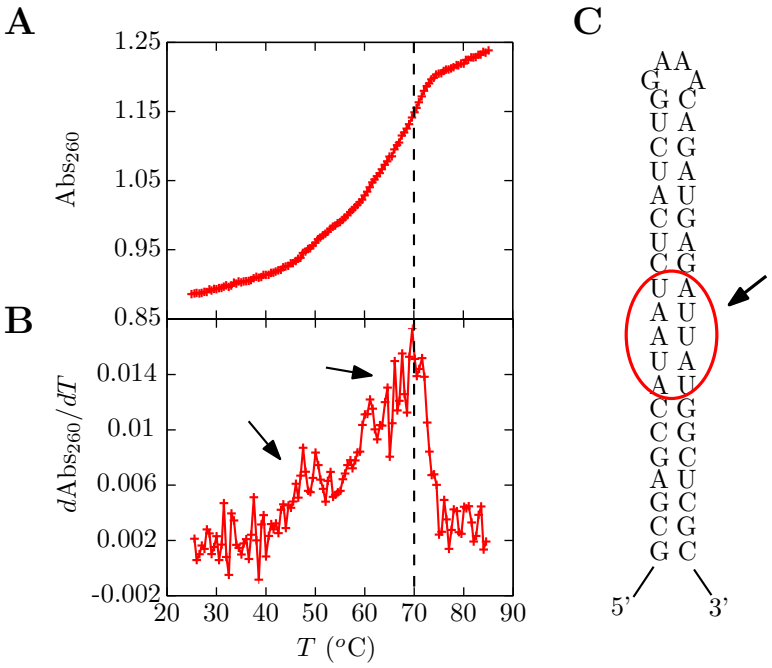

Figure S5: UV Absorbance of the RNA hairpin. **(A)** Experimental results of the absorbance of our RNA hairpin as a function of temperature. **(B)** First derivative of the absorbance as a function of temperature. Its maximum (black dashed line) defines the melting temperature. **(C)** The RNA hairpin under study has a region with a high A-U content in the stem which could lead to premelted states.

We tried to obtain the melting profile adding 100 mM NaCl to the buffer, and the melting temperature was too high and the sample started boiling and evaporating before any relevant signal could be obtained. Therefore, for this RNA hairpin melting curves cannot be measured at the experimental conditions used in our pulling experiments with optical tweezers, and our results can only be compared with Mfold [7, 8, 9] and other theoretical predictions [10, 11, 12]

S6 Rupture force histograms

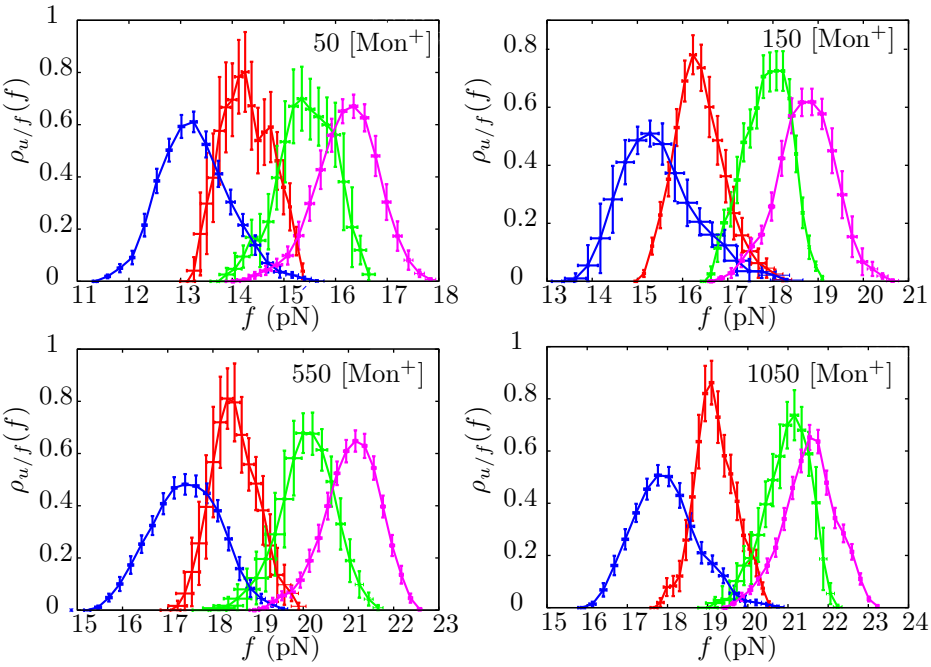

Figure S6: Probability distributions of the unfolding and folding first rupture forces measured at different pulling speeds and different monovalent ionic condition. Red points are folding forces at 1.8 pN/s, green are unfolding forces at 1.8 pN/s, blue are folding forces at 12.5 pN/s and magenta are unfolding forces at 12.5 pN/s.

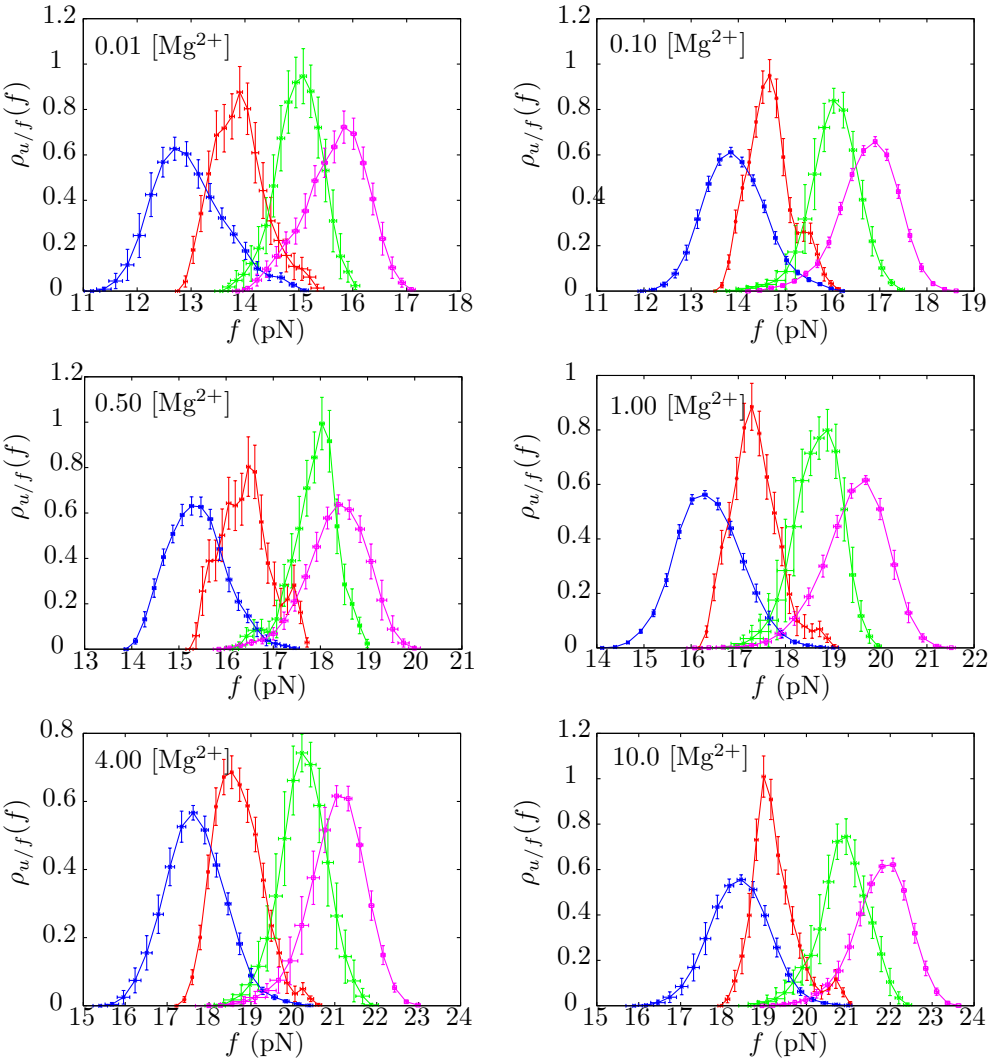

Figure S7: Probability distributions of the first rupture forces measured at different pulling speeds and different magnesium concentration. Red points are folding forces at 1.8 pN/s, green are unfolding forces at 1.8 pN/s, blue are folding forces at 12.5 pN/s and magenta are unfolding forces at 12.5 pN/s.

S7 Tightly Bound Ion Model

In this section the empirical equations of the Tightly Bound Ion (TBI, [11, 12]) model used to predict the hairpin free energies at different ionic conditions are summarized [13, 14].

The external parameters, obtained from the Mfold server [7, 8, 9], are:

Bases in the loop	N_l=4
Bases in the helix	N=20
Hairpin diameter	d=1.7 nm
Interphosphate distance	a=0.6 nm
Enthalpy at 1 M [Mon^+], 0 M [Mg^{2+}]	ΔH_0=199 kcal/mol
Entropy at 1 M [Mon^+], 0 M [Mg^{2+}]	ΔS_0=527.16 mkcal/Kmol

In what follows x is the concentration of monovalent salt and y is the concentration of magnesium ions. Both parameters are given in units of M. Temperature T is given in Celsius.

The empirical set of equations are:

$$\ln Z^l_{Mon}(x) = a^l_1(x)\log(N_l - a/d + 1) + b^l_1(x)(N_l - a/d + 1)^2 - b^l_1(x) \tag{S17}$$

$$\ln Z^c_{Mon}(x) = c^l_1(x)N_l - d^l_1(x) \tag{S18}$$

$$a^l_1(x) = (0.02N_l - 0.026)\log(x) + 0.54N_l + 0.78 \tag{S19}$$

$$b^l_1(x) = \left(-\frac{0.01}{(N_l+1)} + 0.006\right)\log(x) - \frac{7}{(N_l+1)^2} - 0.01 \tag{S20}$$

$$c^l_1(x) = 0.07\log(x) + 1.8 \tag{S21}$$

$$d^l_1(x) = 0.21\log(x) + 1.5 \tag{S22}$$

$$G^l_{Mon}(x) = -(\ln Z^l_{Mon}(x) - \ln Z^c_{Mon}(x)) \tag{S23}$$

$$G^h_{Mon}(x,T) = H_0 - (T + 273.15)S_{Mon}(x)0.001 \tag{S24}$$

$$S_{Mon}(x) = S_0 - 3.22(N-1)g_1(x) \tag{S25}$$

$$g_1(x) = a^h_1(x) + b^h_1(x)/N \tag{S26}$$

$$a^h_1(x) = -0.075\log(x) + 0.012\log^2(x) \tag{S27}$$

$$b^h_1(x) = 0.018\log^2(x) \tag{S28}$$

$$G_{Mon}(x,T) = G^h_{Mon}(x,T) + G^l_{Mon}(x) \tag{S29}$$

$$\ln Z^l_{Mg}(y) = a^l_2(y)\log(N_l - a/d + 1) + b^l_2(y)(N_l - a/d + 1)^2 - b^l_2(y) \tag{S30}$$

$$\ln Z^c_{Mg}(y) = c^l_2(y)N_l - d^l_2(y) \tag{S31}$$

$$a^l_2(y) = \left(-\frac{1}{N_l + 1} + 0.32\right)\log(y) + 0.7N_l + 0.43 \tag{S32}$$

$$b^l_2(y) = 0.0002(N_l + 1)\log(y) - 5.9/(N_l + 1)^2 - 0.003 \tag{S33}$$

$$c^l_2(y) = 0.067\log(y) + 2.2 \tag{S34}$$

$$d^l_2(y) = 0.163\log(y) + 2.53 \tag{S35}$$

$$G^l_{Mg}(y) = -(\ln Z^l_{Mg}(y) - \ln Z^c_{Mg}(y)) \tag{S36}$$

$$\tag{S37}$$

$$G^h_{Mg}(y,T) = H_0 - (T + 273.15)S_{Mg}(y)0.001 \tag{S38}$$

$$S_{Mg}(y) = S_0 - 3.22(N - 1)g_2(y) \tag{S39}$$

$$g_2(y) = a^h_2(y) + b^h_2(y)/N^2 \tag{S40}$$

$$a^h_2(y) = -0.6/N + 0.025\log(y) + 0.0068\log^2(y) \tag{S41}$$

$$b^h_2(y) = \log(y) + 0.38\log^2(y) \tag{S42}$$

$$G_{Mg}(y,T) = G^h_{Mg}(y,T) + G^l_{Mg}(y) \tag{S43}$$

$$x^l_1(x,y) = x/(x + (7.2 - 20/N_l)(40 - \log(x))y) \tag{S44}$$

$$G^l_{Mon,Mg}(x,y) = x^l_1(x,y)G^l_{Mon}(x) + (1 - x^l_1(x,y))G^l_{Mg}(y) \tag{S45}$$

$$G^h_{Mon,Mg}(x,y,T) = H_0 - (T + 273.15)S_{Mon,Mg}(x,y)0.001 \tag{S46}$$

$$S_{Mon,Mg}(x,y) = S_0 - 3.22\left[(N-1)\left(x^h_1(x,y)g_1(x) + (1 - x^h_1(x,y))g_2(y)\right) + g_{1,2}(x,y)\right] \tag{S47}$$

$$x^h_1(x,y) = \frac{x}{x + (8.1 - 32.4/N)(5.2 - \log(x))y} \tag{S48}$$

$$g_{1,2}(x,y) = -0.6x^h_1(x,y)(1 - x^h_1(x,y))\log(x)\log((1/x^h_1(x,y) - 1)x)/N \tag{S49}$$

$$\boxed{G_{Mon,Mg}(x,y,T) = G^h_{Mon,Mg}(x,y,T) + G^l_{Mon,Mg}(x,y)} \tag{S50}$$

Where $G_{Mon,Mg}(x,y,T)$ is the free energy at any temperature and at any monovalent and magnesium ion concentration.

S8 Comparison to the counterion condensation theory

There are two successful theories to account for the energetic interactions between ions in solution and nucleic acids: the Poisson-Boltzmann theory and the counterion condensation theory derived by Manning [10, 15]. These theories are based on different mean field approaches and neglect any kind of correlations between the ions in the solution. More recently a new theory known as the Tightly Bound Ion (TBI) model has been introduced [11], which accounts for the different modes of correlations between counterions.

In Fig. S8 we see the prediction provided by the Manning theory and the TBI model to the free energy of formation of our RNA hairpin as a function of the salt concentration. Because correlations between monovalent ions are negligible, we see that both the Manning theory and the TBI model give similar results under this condition (Fig. S8A). However, correlations between Mg^{2+} are important and the TBI model gives an improved prediction in this case (Fig. S8B) [12].

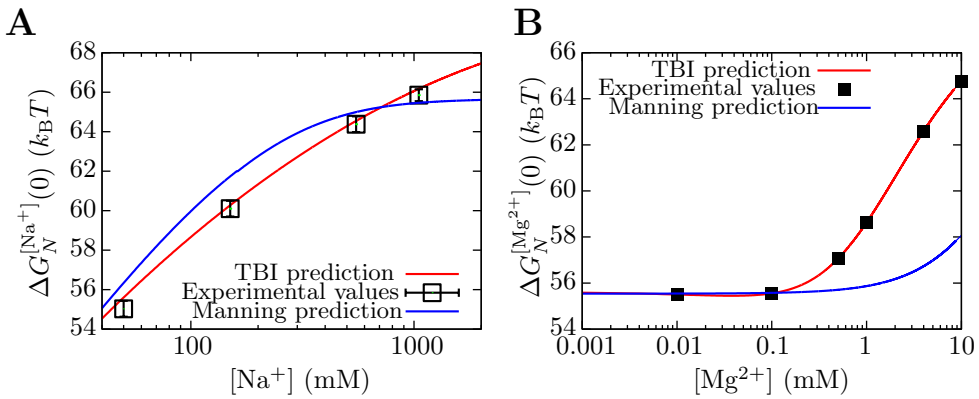

Figure S8: Comparison between experimental data, the counterion condensation theory and the TBI model to predict the behavior of the free energy of formation of our RNA hairpin as a function of salt concentration.

References

[1] Woodside M.T., Anthony P.C., Behnke-Parks W.M., Larizadeh K., Herschlag D. and Block S.M. Direct measurement of the full, sequence-dependent folding landscape of a nucleic acid. Science (2006) 314(5801):1001-4.

[2] Cain R. J. and Glick G. D. (1997) The effect of cross-links on the conformational dynamics of duplex DNA. Nucl. Acids Res. 25(4):836-842.

[3] Sarkar K., Nguyen D. A., Gruebele M. (2010) Loop and stem dynamics during RNA hairpin folding and unfolding. RNA 16(12):2427-2434.

[4] Hyeon, C. and Thirumalai, D. (2007) Measuring the energy landscape roughness and the transition state location of biomolecules using single molecule mechanical unfolding experiments. *J. Phys.: Condens. Matter* **19,** 113101.

[5] Zwanzig, R. (2001) Nonequilibrium Statistical Mechanics, Oxford University Press, 1st edition.

[6] Arrhenius, S. (1889) On the reaction rate of the inversion of non-refined sugar upon souring. *Z Phys Chem* **4,** 226248.

[7] Walter, A. E., Turner, D. H., Kim, J., Lyttle, M. H., Müller, P., Mathews, D. H. and Zuker, M. (1994) Coaxial stacking of helixes enhances binding of oligoribonucleotides and improves predictions of RNA folding. *Proc. Natl. Acad. Sci. U.S.A.*, **91**, 9218-9222.

[8] Mathews, D. H., Sabina, J., Zuker, M. and Turner, D. H. (1999) Expanded sequence dependence of thermodynamic parameters improves prediction of RNA secondary structure. *J. Mol. Biol.*, **288**, 911-940.

[9] Zuker, M. (2003) Mfold server for nucleic acid folding and hybridization prediction. *Nucleic Acids Res.*, **31**, 3406-3415.

[10] Manning, G. S. (1978) The molecular theory of polyelectrolye solutions with applications to the electrostatic properties of polynucleotides. *Q. Rev. Biophys.* **11,** 179-246.

[11] Tan, Z. J. and Chen, S. J. (2005) Electrostatic correlations and fluctuations for ion binding to a finite length polyelectrolyte. *J. Chem. Phys.* **122,** 044903.

[12] Tan, Z. J. and Chen, S. J. (2006) Nucleic Acid Helix Stability: Effects of Salt Concentration, Cation Valence and Size, and Chain Length. *Biophys. J.*, **90**, 1175-1190.

[13] Tan, Z. J. and Chen, S. J. (2007) RNA helix stability in mixed Na^+/Mg^{2+} solution. *Biophys. J.*, **92**, 3615-3632.

[14] Tan, Z. J. and Chen, S. J. (2008) Salt dependence of nucleic acid hairpin stability. *Biophys. J.*, **95**, 738-752.

[15] Manning, G. S. (2002) Electrostatic free energy of the DNA double helix in counterion condensation theory. *Biphys. Chem.* **101-102,** 461-473.